3D printed carbon-fibre reinforced composite lattice structures with good thermal-dimensional stability

Yuan Chen[1,2], Lin Ye[1,2*], Anthony J. Kinloch[1,3], Y.X. Zhang[4]

[1]Centre for Advanced Materials Technology (CAMT), School of Aerospace, Mechanical and Mechatronic Engineering, The University of Sydney, NSW 2006, Australia

[2]School of System Design and Intelligent Manufacturing (SDIM), Southern University of Science and Technology, Shenzhen, China

[3]Department of Mechanical Engineering, Imperial College London, South Kensington Campus, London SW7 2AZ, UK

[4]School of Engineering, Western Sydney University, NSW 2751, Australia

Abstract

A good dimensional stability is a crucial property of any base-platform structure for the attachment of high precision optical or mechanical devices, such as imaging equipment, satellite antennas, thermal sensors, etc., where the surrounding temperature may fluctuate substantially. The present study demonstrates how such a base-platform in a form of a dual-composite, planar-lattice structure can be designed and rapidly, and conveniently, manufactured using 3D printing via fused filament fabrication (FFF). Specifically, the planar-lattice consists of a central cross-lattice manufactured using a continuous carbon-fibre reinforced polyamide (CCF/PA) composite with four interlocking outer-strips manufactured using a short carbon-fibre reinforced polyamide (SCF/PA) composite. Numerical finite-element analyses of the planar-lattices are developed, and validated by experimental results, with respect to their thermal-deformation behaviour. This numerical analysis is then used to study the effects of various types of fibre architecture for the composites that might be used to manufacture the planar-lattice. The results demonstrate, for the first time, the ability of 3D printing, using FFF, to manufacture base-platform structures which use dual-composite materials, based upon carbon-fibre reinforced polyamide materials, in order to achieve a very good thermal-dimensional stability.

Keywords: Thermal-dimensional stable structures; 3D printing; CF/PA composites; finite-element analysis; coefficient of thermal expansion (CTE); fused filament fabrication (FFF).

* Corresponding author: E-mail addresses: lin.ye@sydney.edu.au

1. Introduction

A high thermal-dimensional stability is a crucial property of any base-platform structure for the attachment of high precision optical or mechanical devices, such as imaging equipment, satellite antennas, thermal sensors, etc., where the surrounding temperature may fluctuate substantially. To attain a good thermal-dimensional stability, it is recognised that a near-zero value of the effective coefficient of thermal expansion (CTE) for the base-platform structure is highly desirable [1][2][3].

This requirement of a near-zero effective CTE for the base-platform is typically met by the design of macroscale lattice-structures manufactured using dual-material components [4][5][6][7][8][9][10]. The dual-materials employed are usually two dissimilar isotropic polymers or metals. However, several important aspects of such dual-material, macroscale lattice-structures have yet to be studied in detail. The first is the ease and cost of manufacturing such planar-lattice structures and recent developments in 3D printing via the fused filament fabrication (FFF) method would suggest that such 3D printing offers significant benefits in these respects [11][12][13][14]. Secondly, it is well established that anisotropic composites, such as continuous carbon-fibre reinforced polymers, can offer improved mechanical properties compared to their isotropic counterparts [15]. Furthermore, carbon fibres have a negative CTE [16][17] and when carbon fibres are present in a polymeric matrix, which normally possesses a positive CTE, the carbon-fibre polymeric-matrix composite can be tailored, in principle, to have an almost zero CTE in the fibre axial direction. Indeed, several authors [18][19] have reported theoretical studies on the fibre architecture needed for producing fibre-polymer composites with a zero, or near-zero, CTE. Thus, carbon-fibre polymer-matrix composites would appear to be very useful materials for producing components which can be designed to possess a good thermal-dimensional stability.

The present study aims to design and manufacture a base-platform structure in the form of a dual-composite planar-lattice with continuous and/or short carbon-fibre composites using 3D printing based upon the fused

filament fabrication (FFF) method. Numerical finite-element analyses, validated by experimental results, of the planar-lattices are developed to describe their thermal-deformation behaviour. The effects of the various types of fibre architecture that might be used to manufacture the planar-lattice will then be assessed. Thereby, the intention is to identify the design of a 3D FFF printed, planar-lattice structure, manufactured using dual-materials based upon carbon-fibre reinforced polyamide composites, which possesses a very good thermal-dimensional stability.

2. Experimental studies

2.1 Design of lattice configurations

A dual-composite, planar-lattice structure, based on a design with a dual-material triangular CTE mechanism previously reported in the literature [2], was designed to act as a potential base-platform structure possessing a relatively low effective CTE. The main design that was investigated is shown in Figure 1. The planar-lattice consisted of a central cross-lattice of a continuous carbon-fibre (CCF) reinforced polyamide 6 (PA6), termed a CCF/PA composite, and four outer-strip components of a short carbon-fibre (SCF) reinforced polyamide 6 (PA6) matrix, termed a SCF/PA composite. Both the central cross-lattice and the four outer-strips clearly needed to be joined together and a relatively tight, push-fit, interlock mechanism was adopted [9], see Figure 1.

In principle, the unidirectional CCF composites possess a very low CTE in the fibre direction, but the CTE in the transverse direction is relatively high. Thus, with a structure made of solely unidirectional CCFs it is difficult to achieve thermal-dimensional stability in all directions. In addition, a unidirectional CCF composite is susceptible to delamination due to its relatively low fracture resistance in the transverse direction. However, a woven or cross-ply CCF composite can usually eliminate the strong anisotropy observed in the values of the CTE, resulting in an orthotropic composite with a comparatively low overall CTE, i.e. below approximately 5×10^{-6}/°C [18][19][20]. Therefore, a configuration with a lay-up of 45°/135° for the CCF/PA composite, in

the global coordinates, was adopted for the central cross-lattice for the planar-lattice structure. This design gives eight legs with a near cross-ply configuration with respect to their local coordinates. The four outer-strips were manufactured using the SCF/PA composite since it possesses better mechanical properties than pure PA6. The SCF/PA outer-strips were also printed using a 45°/135° architecture, since orientation of the SCFs has been shown [20] to occur upon the filaments being deposited during the FFF process.

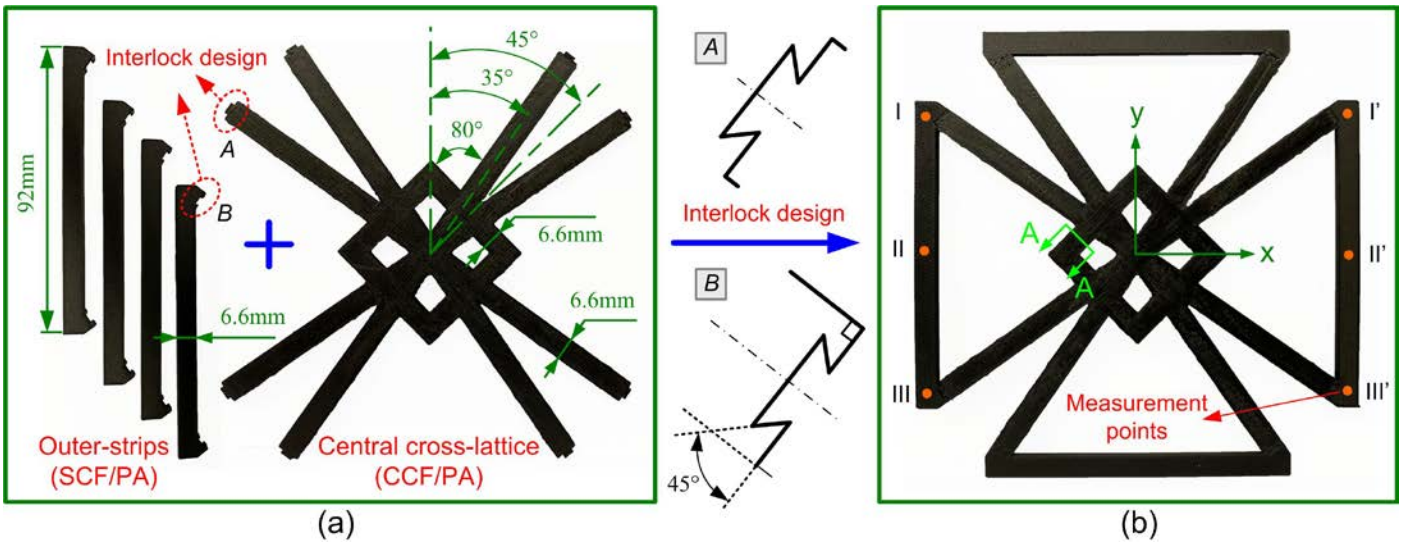

Figure 1. Components of the main dual-composite, planar-lattice structure studied: (a) the 3D printed CCF/PA central cross-lattice and four SCF/PA outer-strips, with a tight-fit geometric interlock, to form (b) the dual-composite CF/PA planar-lattice. (Note that *y*-*x* is the global coordinate system and A-A shows the direction for the optical cross-section micrograph shown below in Figure 4(a). The positions I-I', II-II' and III-III' were used for the determination of the thermal displacements.)

2.2 The materials and the FFF process

All the components of the planar-lattice structure were manufactured by 3D printing, via the FFF process, using a desktop 3D printer (Markforged® Mark Two, USA). For the CCF/PA composite the feedstock was filaments of 34 vol% of CCFs in a PA6 matrix and for the SCF/PA composite the feedstock was filaments of 10 vol% of SCFs in a PA6 matrix, both supplied by Markforged®, USA. The SCFs had a mean length of 105 µm. The default, i.e. pre-set, printing parameters were used with the temperature set at 275°C and a deposition

speed of 16 mm/s. The diameter of the extruded filaments of the composites was approximately 0.4 mm before deposition. When the central cross-lattice was manufactured using the CCF/PA composite, sixteen filament layers of the CCF/PA, in an architecture of $[45°/135°]_8$, were deposited, as shown in Figure 2, with the 45° and 135° directions being defined with respect to the lengthwise direction of the legs of the cross-lattice. Additional top and bottom surface layers were then printed using a single layer of the SCF/PA composite to give a better surface appearance, which aided the digital image correlation (DIC) studies for measuring the thermal deformation. The architecture for the deposition of layers of the CCF/PA composite of a fibre lay-up of $[45°/135°]_8$ for the central cross-lattice was selected based upon a consideration of the best balance of mechanical properties coupled with its relatively low CTE in the two diagonal directions. The SCF/PA outer-strips were also printed with a $[45°/135°]_9$ architecture, with the 45° and 135° directions being defined with respect to the lengthwise direction of the legs of the outer-strip components.

In order to investigate any beneficial effects of using the dual-composite approach, some planar-lattices were also fabricated using the 3D FFF printing process but now employing solely the SCF/PA composite for all the various components, i.e. for both the central cross-lattice and the four outer-strips. For such SCF/PA planar-lattices, eighteen layers of the SCF/PA composite were deposited using a $[45°/135°]_9$ architecture. Therefore, for all the 3D printed components manufactured using the FFF printing process, eighteen layers of the appropriate composite were deposited to give a final thickness of each component of nominally 2.25 mm.

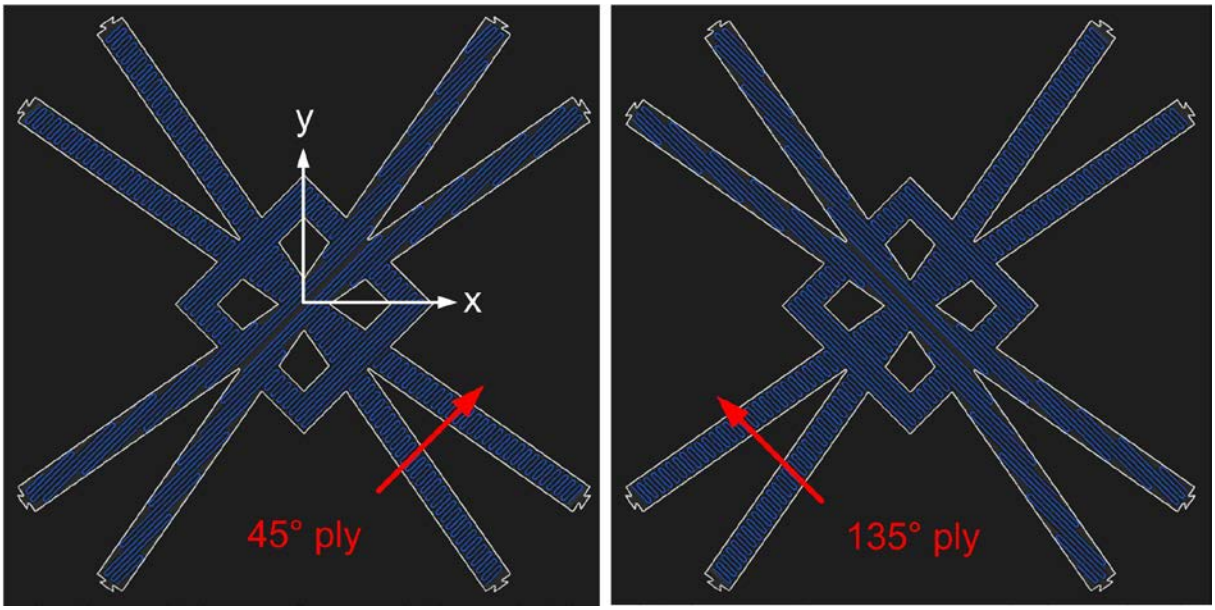

Figure 2. Deposition trajectories in an alternate 45°/135° approach for the 3D-printed CCF/PA central cross-lattice.

2.3 CTE measurements and DIC photographic analysis

The planar-lattices were subjected to an increasing test temperature, from room temperature, using a heating-plate, capable of maintaining a given temperature to within an accuracy of ± 0.2℃, and employing a heating rate of approximately 2℃/s. For monitoring the temperature at various positions on the planar-lattices, as indicated in Figure 1(b), a thermal camera was used, as shown in Figure 3. The testing environment was a nominal humidity of approximately 60% and room temperature was 20℃. The planar-lattices were heated from room temperature up to 81℃, which was the maximum temperature that could be reliably achieved.

To measure the displacements, i.e. the lateral movements, induced by an increase in the temperature of the components forming the planar-lattice, a digital image correlation (DIC) technique was employed. For the DIC analysis a white-coloured coating was sprayed onto the surface of the planar-lattice followed by the application of a uniform pattern of black-dots, which were applied using an embossed ink-covered roller. These black-dots could be captured by the DIC camera to enable the determination of the displacements at the various positions marked on the outer-strip components of the planar-lattice, see Figure 1(b). Due to the same response in the *x*- and *y*-directions of the planar-lattice, which arises from (a) the symmetry of its design and

(b) the use of the symmetric 45°/135° architecture for the CCF/PA and SCF/PA composites when used to manufacture the central cross-lattice component and four outer-strip components, only the thermal displacements of the planar-lattice in the *x*-direction were measured. (Note that the origin of the *x*- and *y*-axes was taken to be the centre point of the central cross-lattice, see Figure 1(b).) The analysis of the DIC measurements was undertaken using an open-source 'Ncorr Matlab' software, where the accuracy of the measured displacement was determined by using a least-square plane fitting method and the details of this procedure can be found in [21].

2.4 Analysis of the thermal behaviour and the determination of the CTE

Again, due to the same response in the *x*- and *y*-directions of the planar-lattice, in the following discussions only the behaviour of the planar-lattice in the *x*-direction is considered. To analyse the thermal behaviour and to measure the effective CTE, i.e. the overall CTE of the planar-lattice structure, DIC photographic analysis was employed and the equation used for calculating the effective CTE, α_i, at a temperature, T_i, was:

$$\alpha_i = \frac{\varepsilon_i^{th}}{T_i - T_0} \tag{1}$$

where ε_i^{th} is the effective thermal strain, measured using the DIC analysis, at the various measurement positions shown in Figure 1(b), taking an average value for the positions I-I', II-II' and III-III', at a temperature T_i with a reference temperature, T_0, which was 20°C. Thus, the effective CTE, α_e, to assess the thermal-dimensional stability can be calculated from:

$$\alpha_e = \frac{\sum_{i=1}^{n} |\alpha_i|}{n} \tag{2}$$

where *n* is the total number of the various temperatures at which measurements were taken.

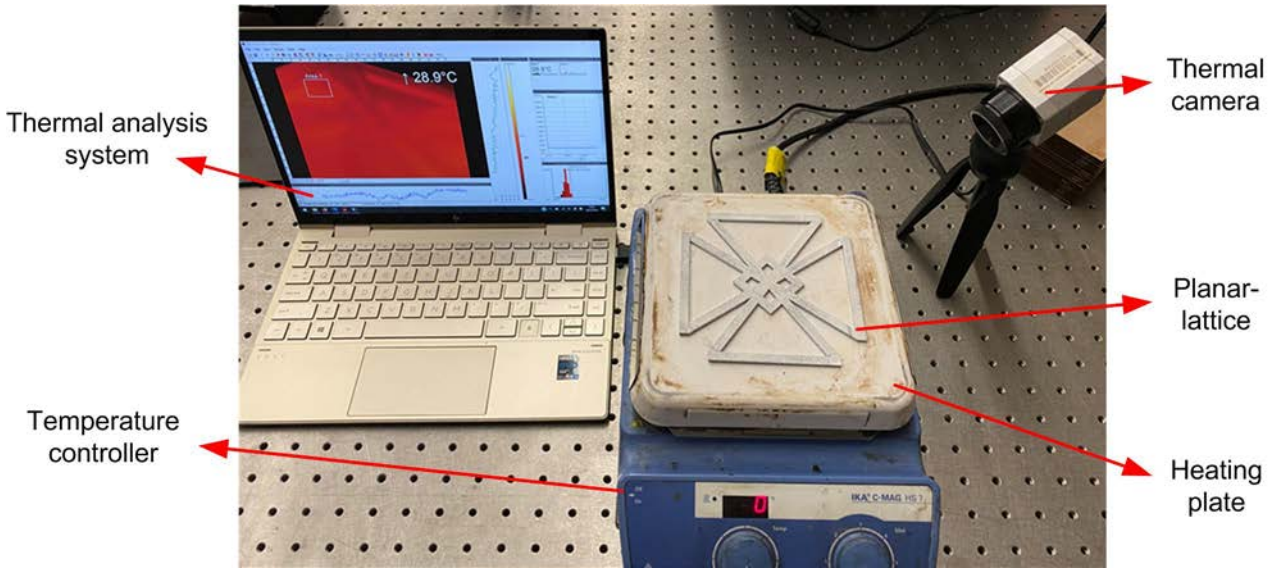

Figure 3. Experimental set-up for measuring the thermally-induced displacements and hence deducing the effective CTE of the composite planar-lattice structures.

3. Numerical analysis

3.1 The finite-element analysis (FEA) numerical model

A finite-element analysis (FEA) numerical model was developed using the Abaqus Standard [22] code to calculate the predicted displacements of the composite planar-lattice structures as a function of the test temperature. Essentially, the planar-lattices were modelled using continuum shell elements of eighteen layers, as shown in Figure 4. These elements were 8-noded, thermally-coupled, quadrilateral, in-plane, general-purpose continuum shells with reduced integration ('SC8RT'), which were specified on 3D solid-elements but behaved similarly to conventional shell elements in terms of their kinematic and constitutive behaviour. This resulted in an accurate model for the stacked composite plies [23] and which allowed the through-thickness response to be determined [22]. An element size of 1 mm was used to model the central cross-lattice and the four outer-strip components which form the planar-lattice, following convergence and mesh-independence studies. A general contact algorithm was applied to calculate the common interactions at the interlocking points. The model was implemented using the penalty and hard-contact methods for the general contacts, with

a friction coefficient of 0.3 [14].

Thermo-elastic models were developed using the orthogonal linear-elastic constitutive relations for each layer of 3D printed CCF/PA and SCF/PA composites, based on their known linear-elastic and thermal properties. The properties of the CCF/PA and SCF/PA composites used for the modelling studies of the components of the planar-lattices are given in Table 1. Basically, the constitutive stress versus strain relation could be calculated under a material Cartesian coordinate system, as a function of both the elastic modulus and the thermal strain, as follows:

$$\boldsymbol{\sigma} = \boldsymbol{E}\boldsymbol{\varepsilon}^{th} \tag{3}$$

where $\boldsymbol{\sigma}$ is the stress vector, $\boldsymbol{E}$ is the stiffness matrix, and $\boldsymbol{\varepsilon}^{th}$ is the thermal-strain vector produced by thermal expansion of the composite. This can be expressed by:

$$\boldsymbol{\varepsilon}^{th} = \int_{T_0}^{T_i} \boldsymbol{\alpha} dT_i \tag{4}$$

where $\boldsymbol{\alpha}$ is the vector of the orthogonal CTE properties, and T_i and T_0 are the current and the reference temperatures, respectively.

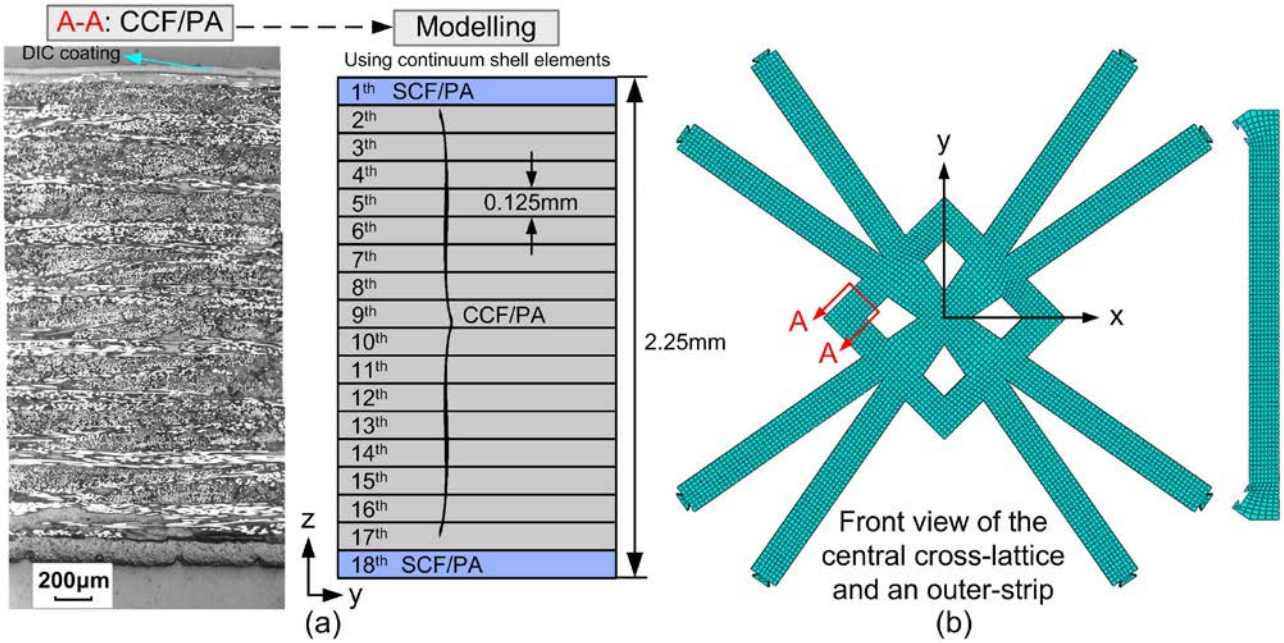

Figure 4. (a) An optical micrograph of the cross-section of the CCF/PA central cross-lattice with the corresponding model and (b) a front view showing the FEA mesh implemented for the central cross-lattice and an outer-strip.

3.2 The mechanical and thermal properties of the CCF/PA and SCF/PA composites

The mechanical and thermal properties of the unidirectional CCF/PA and SCF/PA composite materials needed to undertake the numerical analyses were either directly measured or taken from the literature. The values employed are given in Table 1.

Table 1. Elastic and thermal properties of unidirectional layers CCF/PA and SCF/PA.

Description	Variable	CCF/PA	Ref.	SCF/PA	Ref.
Density (kg/m^3)	ρ	1250	[24]	1160	[12]
Fibre volume content (%)	V_f	31.4	[24]	10.0	[14]
Longitudinal elastic modulus (GPa)	E_1	69.4	[24]	1.4	+
Transverse elastic modulus (GPa)	E_2	3.5	[24]	0.6	+
Shear elastic modulus (GPa)	G_{12}	1.9	[24]	0.31	+
Poisson's ratio	ν_{12}	0.33	[25]	0.39	+
Longitudinal CTE (10^{-6}/°C)	α_1	6.53	+	66.2	+
Transverse CTE (10^{-6}/°C)	α_2	59.0	+	86.0	+
Thermal conductivity (mW/mm/°C)	k	2.97	[26]	0.27	[26]
Specific heat (J/kg/°C)	C_p	768	+	848	[27]

Note: + signifies determined in the present work.

4. Results and Discussion

4.1 The measured and predicted thermal displacements, U_{xx}, in the planar-lattice structures

The thermal displacements, U_{xx}, i.e. lateral movement, in the x-direction, as a function of the test temperature, as measured from the experiments and predicted from the numerical simulations, are shown in Figures 5 and 6 for the two planar-lattice structures which were 3D printed. (In these figures the origin is taken to be the centre of the central cross-lattice, see Figure 1(b)). In Figure 5 the results are shown for a dual-composite planar-lattice consisting of a CCF/PA central cross-lattice component and four SCF/PA outer-strip components. Whilst, in Figure 6, the composite planar-lattice consists, instead, of a SCF/PA central cross-lattice component and four SCF/PA outer-strip components, and was therefore 3D printed using solely the SCF/PA composite.

Several interesting points emerge from these results.

Firstly, in both Figures 5 and 6 there is clearly a good agreement between the experimental and the numerical modelling results. This good agreement is most clearly revealed in Figure 6, since for this type of planar-lattice manufactured solely using the SCF/PA composite, the thermal displacements, U_{xx}, of the outer-strips are significantly greater and therefore represent a greater challenge for the numerical studies. Thus, the numerical simulations clearly give valid results.

Secondly, from Figures 5 and 6, it may be seen that, as the temperature is increased, the solely SCF/PA planar-lattice, as shown in Figure 6, undergoes larger thermal displacements, U_{xx}, than the planar-lattice which is manufactured using the CCF/PA composite for the central cross-lattice and the SCF/PA composite for the four outer-strips, as shown in Figure 5. Thus, the thermally-induced deformations are significantly reduced for the planar-lattice with a CCF/PA central cross-lattice component and four SCF/PA outer-strip components, compared to the solely SCF/PA planar-lattice. Indeed, the thermal deformations are almost negligible for the planar-lattice which has been 3D printed using the FFF process employing the dual-composites of the CCF/PA and SCF/PA materials, see Figure 5.

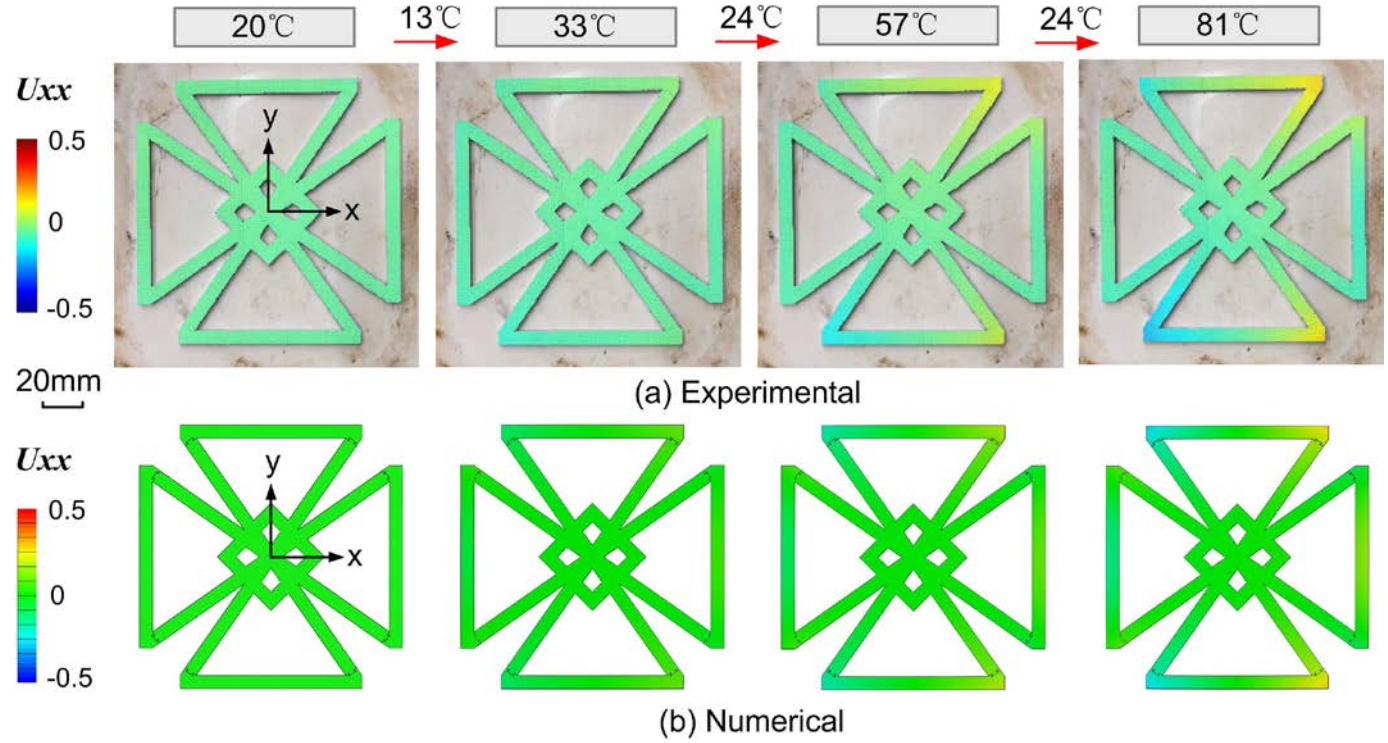

Figure 5. Thermal displacements, U_{xx}, of a dual-composite planar-lattice structure consisting of a CCF/PA central cross-lattice component and four SCF/PA outer-strip components as a function of temperature: (a) experimental measurements and (b) numerical predictions.

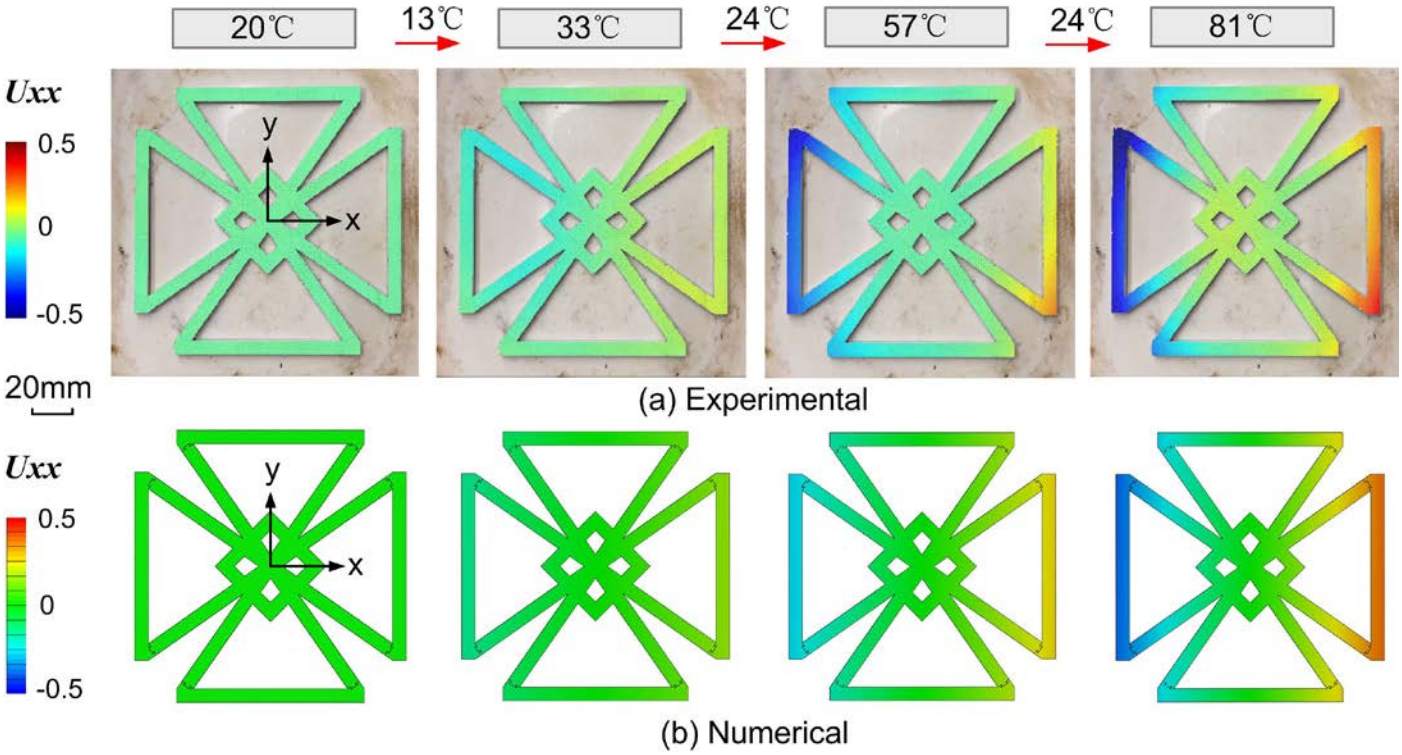

Figure 6. Thermal displacements, U_{xx}, of a composite planar-lattice structure consisting of a SCF/PA central cross-lattice component and four SCF/PA outer-strip components as a function of temperature: (a) experimental measurements and (b) numerical predictions.

4.2. The coefficient of thermal expansion of the planar-lattice structures

Based on Equations (1) and (2), and using the measurement positions shown in Figure 1(b), the effective CTEs, α_e, in the x-y global coordinates versus the test temperature of the planar-lattices, were determined and are shown in Figure 7, where the values predicted from the numerical modelling studies are also included. It may be seen that the values of the effective CTE versus the test temperature from both the direct experimental measurements and the numerical modelling studies are in very good agreement. For example, firstly, the planar-lattices with a CCF/PA central cross-lattice component and four SCF/PA outer-strip components have an effective CTE of 4.6×10^{-6}/°C from the direct experimental measurements and 5×10^{-6}/°C from the numerical simulations. Secondly, the effective CTE, α_e, calculated using Equation (2) for the solely SCF/PA planar-lattices from the experimental measurements is 75×10^{-6}/°C, whilst that calculated from the numerical simulation is 72.8×10^{-6}/°C. Thus, again, the numerical simulations clearly give valid results.

Comparing the two types of composite planar-lattices examined in the present study, the effective CTE of the planar-lattice using a CCF/PA central cross-lattice component and four SCF/PA outer-strip components, see Figure 7(a), is approximately only 6.5% of that shown by the planar-lattice using solely SCF/PA components. These values again clearly demonstrate the significant enhancement in the thermal-dimensional stability given by the dual-composite planar lattice, compared to that using solely the SCF/PA composite.

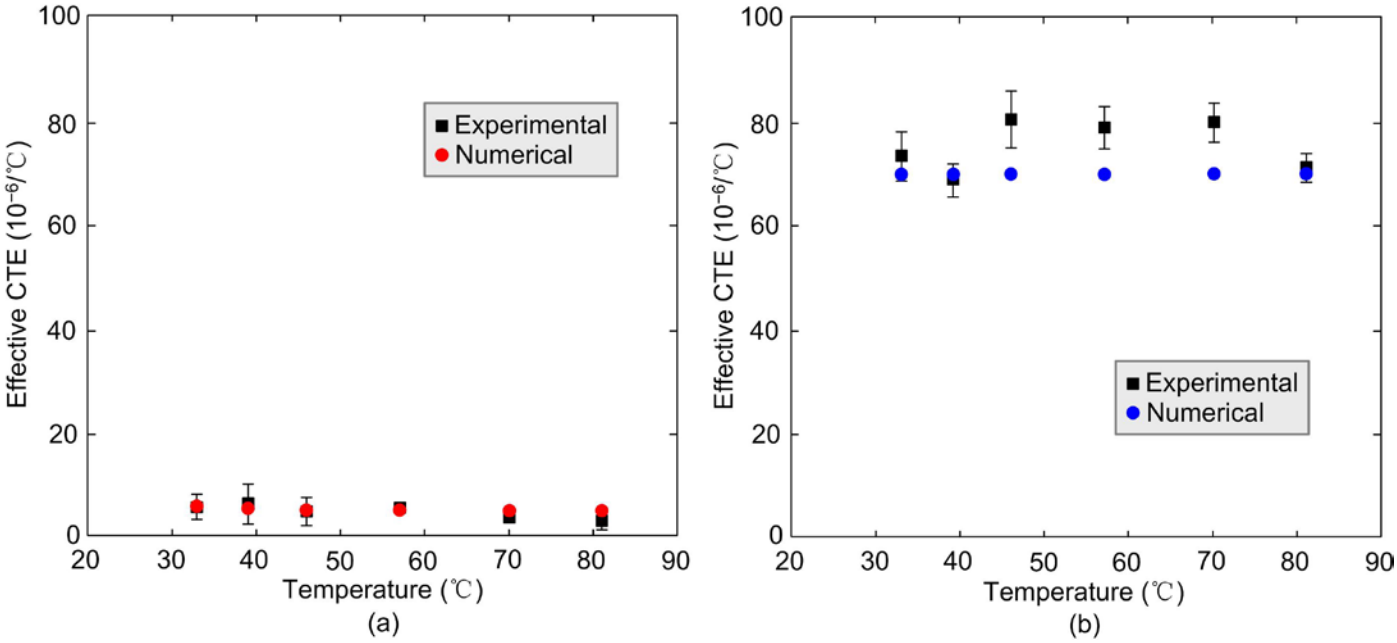

Figure 7. Experimental and numerical results of the effective CTE, α_e, versus the test temperature of the composite planar-lattice structures: (a) with a CCF/PA central cross-lattice component and four SCF/PA outer-strip components, and (b) with a SCF/PA central cross-lattice component and four SCF/PA outer-strip components. (The experimental error bars represent +/− one standard deviation.)

4.3. Thermally-induced strains and stresses in the planar-lattice structures

Figure 8 depicts the thermal strains, ε_{xx}, and von Misses stresses in the *x*-direction, calculated from the numerical FEA modelling studies, at the reference temperature of 20℃ and at 81℃, present in the first layer of the two types of composite planar-lattices. From Figure 4, it may be seen that, for both of these planar-lattices, this first layer consists of the SCF/PA composite.

Firstly, at the reference temperature of 20℃, there are no significant strains and stresses present, see Figure 8(a). Secondly, however, for the dual-composite planar-lattice, consisting of the CCF/PA central cross-lattice component and four SCF/PA outer-strip components of strips, at 81℃, see Figure 8(b), the higher CTE of the SCF/PA composite forces the connecting legs of the CCF/PA central cross-lattice frame to bend outwards with an angle increment of about 0.1°. In contrast, the cross-lattice of the solely SCF/PA planar-lattice at 81℃ shows generally higher strains and no angle increment is observed to occur, see Figure 8(c). Now, this change in the angle of 0.1° might seem to be insignificant for the dual-composite planar cross-lattice consisting of the CCF/PA central cross-lattice component and four SCF/PA outer-strip components. Nevertheless, it leads to a

significant improvement in the thermal-dimensional stability of the planar-lattice, as will be discussed in the following section. Finally, as shown in Figure 8(b), at 81°C the planar-lattice consisting of a CCF/PA central cross-lattice component and four SCF/PA outer-strip components has higher stresses present than the planar-lattice using solely the SCF/PA composites, see Figure 8(c). Indeed, this result is to be expected, since the dual-composite planar-lattice consisting of a CCF/PA central cross-lattice component and four SCF/PA outer-strip components is constrained so as to give small thermal displacements and hence a low effective CTE. However, this leads to the build-up of stresses in the central cross-lattice, compared to that when solely SCF/PA composites are used in the manufacture of the planar-lattice, as may be seen from comparing Figures 8(b) and 8(c). However, the magnitude of the stresses so developed are only about 10 MPa, as shown in Figure 8(b), which are relatively low in value and are in the linear-elastic range for these composite materials.

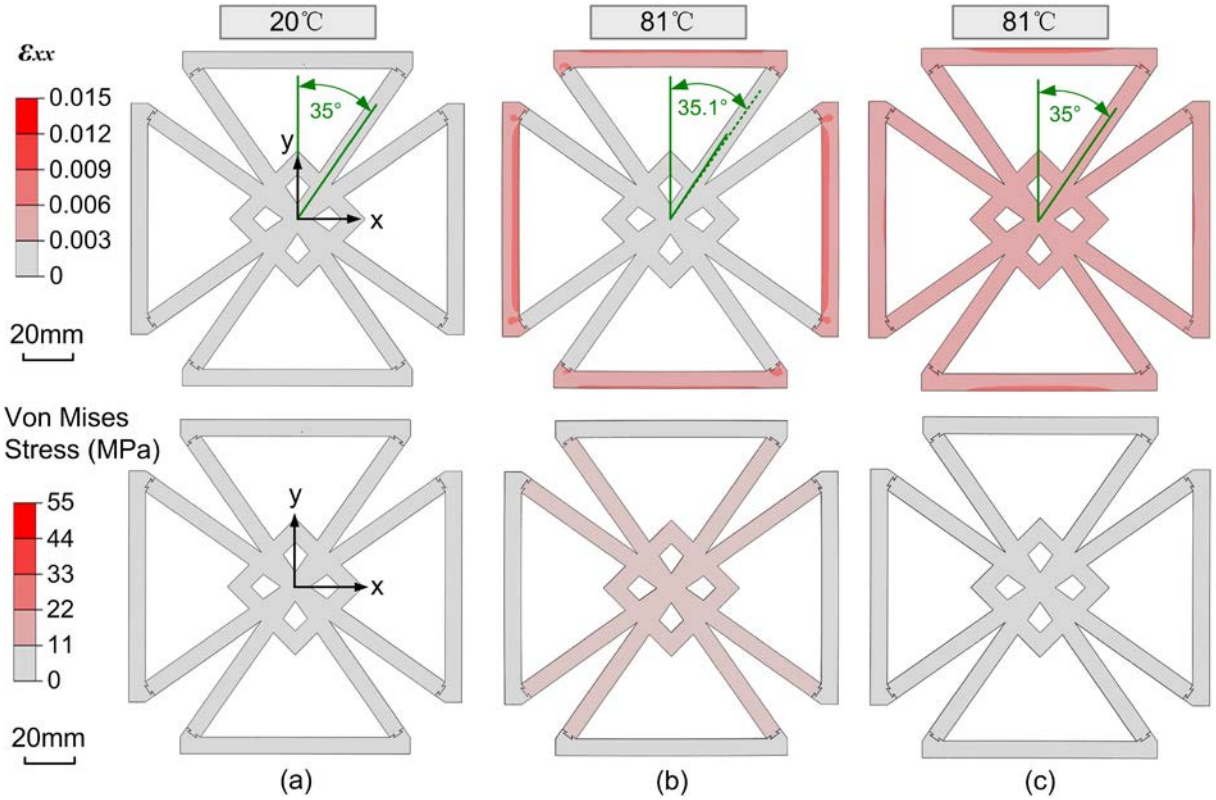

Figure 8. The thermal strains, ε_{xx}, and von Mises stresses in the *x*-direction in the first layer of composite material. Firstly, (a) for both types of composite planar-lattice structures when at the reference test temperature of 20°C. Secondly, (b) at 81°C for a CCF/PA central cross-lattice component and four SCF/PA outer-strip components. Thirdly, (c) at 81°C for a SCF/PA central cross-lattice component and four SCF/PA outer-strip components, i.e. using solely the SCF/PA composite. (Note: for both types of cross-lattice structures, the first layer of composite is a layer of the SCF/PA material.)

4.4. The dual-composite material approach

In the design of the planar-lattice that is based upon a dual-composite materials approach of the CCF/PA central cross-lattice and the SCF/PA four outer-strips, then two mechanisms lead to the good thermal-dimensional stability of this type of dual-composite planar-lattice.

The first mechanism arises from using the CCF/PA composite to manufacture the central cross-lattice. Essentially, this mechanism results from the thermal expansion that occurs with an increase in temperature being modulated by the cross-diagonal legs of the central cross-lattice being manufactured using the CCF/PA composite that possesses a relatively low CTE, compared to the SCF/PA. Thus, a relatively low value of the effective CTE for the planar-lattice structure is observed.

In addition, there is a second mechanism that arises from the interaction between the two different composites used for the central cross-lattice and the outer-strip components which further reduces the thermal expansion, and hence the value of the CTE, for the dual-composite planar-lattice, as shown schematically in Figure 9. This arises from employing a central cross-lattice manufactured using the CCF/PA, which possesses a relatively low CTE, but manufacturing the outer-strips using the SCF/PA composite which has a significantly higher CTE. Indeed, the results from the numerical modelling studies predicted that, at a temperature of 81°C, for the planar-lattice manufactured using this dual-composite approach that (a) a change in the angle of the diagonal leg of the cross-lattice of about 0.1° would occur and (b) the effective CTE would be 5×10^{-6}/°C. (It should be noted that this predicted value of the effective CTE is in excellent agreement with the experimentally measured value, see Figure 7(a).) On the other hand, for a planar-lattice made of solely the CCF/PA composite it was predicted that, at 81°C, (a) there would be no change in the angle of the diagonal leg of the cross-lattice and (b) the effective CTE would now be clearly greater in value at 10×10^{-6}/°C. Thus, this second 'interaction mechanism' that arises from using the dual-composite approach for the 3D printing of the planar-lattice structure gives a further reduction of about 50% in the effective CTE for the dual-composite planar-lattice.

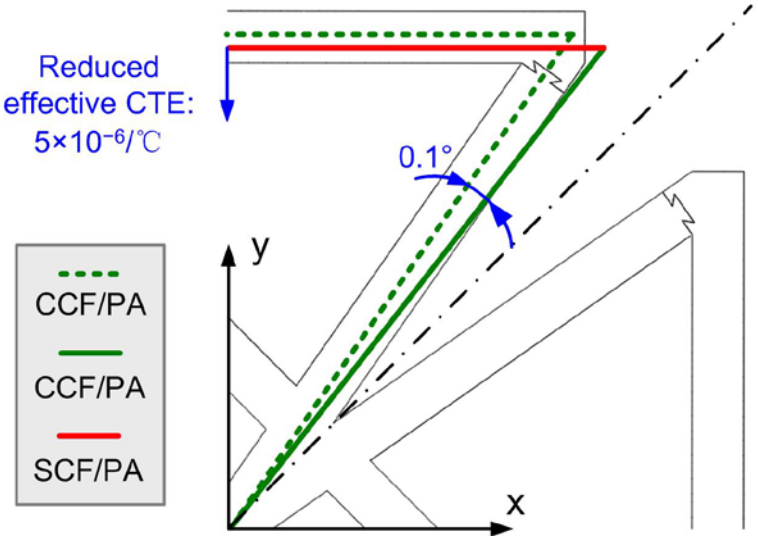

Figure 9. The 'interaction mechanism' for obtaining a reduced effective CTE, which is active in dual-composite planar-lattice structures.

5. Conclusions

There is a need for base-platform structures, which are used for the attachment of high precision optical or mechanical devices, such as imaging equipment, satellite antennas, thermal sensors, etc., to possess very good thermal-dimensional stability when the surrounding temperature may fluctuate substantially. The present study has demonstrated how such a base-platform in the form of a planar-lattice structure may be rapidly and conveniently manufactured using 3D printing via the fused filament fabrication (FFF) method. The designs of the planar-lattices were based on using carbon-fibre reinforced polyamide composites to manufacture a central cross-lattice with four outer-strip components. The central cross-lattice and the four outer-strips clearly needed to be joined together and a relatively tight push-fit interlock design was adopted. Numerical finite-element analyses, validated by experimental measurements, of the various designs of planar-lattices have been developed (a) to describe their thermal-deformation behaviour and (b) to study the effects of various types of fibre architecture for the composites used for the central cross-lattice.

The design of the 3D FFF printed planar-lattice structure which resulted in the superior thermal-dimensional stability was a novel dual-composite material design and possessed a central cross-lattice manufactured using

a continuous carbon-fibre reinforced polyamide (CCF/PA) composite, with four interlocking outer-strip components manufactured using a short carbon-fibre reinforced polyamide (SCF/PA) composite. The central cross-lattice was printed by depositing sixteen filament layers of the CCF/PA, in an architecture of [45°/135°], with additional top and bottom surface layers being printed using a single layer of the SCF/PA composite. The outer-strips were printed using eighteen filament layers of SCF/PA composite which were also deposited in an architecture of [45°/135°]. This new design using a dual-composite, planar-lattice structure possessed an effective coefficient of thermal expansion (CTE), as measured experimentally and as predicted from the numerical analyses, of only about 6.5% of that shown by a similar design but which solely used SCF/PA printed components. Indeed, the dual-material design of the planar-lattice structure had a very low value of the effective CTE of 4.6×10^{-6}/°C from the direct experimental measurements and of 5.0×10^{-6}/°C from the numerical simulations.

Therefore, these results demonstrate, for the first time, the ability of 3D printing using the FFF method to manufacture base-platform structures, which are dual-material in nature and are based upon carbon-fibre reinforced polyamide composites planar-lattices, in order to achieve a very good thermal-dimensional stability. Finally, it should be noted that a main aim of the current study has been to propose and develop a dual-composite lattice with good thermal-dimensional stability from a two-dimensional viewpoint, without considering the third dimension where out-of-plane loading conditions need to be taken into account. Studies are currently on-going of such dual-composite structures, manufactured using the FFF process, with the aim of optimising the design to achieve very good thermal-dimensional stability from a three-dimensional viewpoint.

Acknowledgements

The authors would like to thank the Australian Research Council for financial support via a Discovery Project Grant (DP190102354) and they are also grateful for the support of the School of Aerospace, Mechanical and Mechatronic Engineering (AMME), the University of Sydney.

References

[1] Tenney DR, Tompkins SS, Sykes GF. Proceedings of 'Large Space Antenna Systems Technology' Conference, NASA Langley, USA. December 4-6, 1984, p. 301-30.

[2] Miller W, Mackenzie DS, Smith CW, Evans KE. A generalised scale-independent mechanism for tailoring of thermal expansivity: Positive and negative. Mech Mater 2008; 40: 351–61.

[3] Jefferson G, Parthasarathy TA, Kerans RJ. Tailorable thermal expansion hybrid structures. Int J Solids Struct 2009; 46: 2372–87.

[4] Lehman J, Lakes RS. Stiff, strong, zero thermal expansion lattices via material hierarchy. Compos Struct 2014; 107: 654–63.

[5] Lakes RS. Cellular solid structures with unbounded thermal expansion. J Mater Sci 1996; 15: 475–77.

[6] Lakes RS. Cellular solids with tunable positive or negative thermal expansion of unbounded magnitude. Appl Phys Lett 2007; 90: 221905.

[7] Takezawa A, Kobashi M. Design methodology for porous composites with tunable thermal expansion produced by multi-material topology optimization and additive manufacturing. Compos Part B Eng 2017; 131: 21–9.

[8] Steeves CA, dos Santos e Lucato SL, He M, Antinucci E, Hutchinson JW, Evans AG. Concepts for structurally robust materials that combine low thermal expansion with high stiffness. J Mech Phys Solids 2007; 55: 1803–22.

[9] Wei K, Chen HS, Pei YM, Fang DN. Planar lattices with tailorable coefficient of thermal expansion and high stiffness based on dual-material triangle unit. J Mech Phys Solids 2016; 86: 173–91.

[10] Yu HB, Liang B, Zhao ZF, Liu PP, Lei HS, Song WL, Chen MJ, Guo XG. Metamaterials with a controllable thermal-mechanical stability: Mechanical designs, theoretical predictions and experimental demonstrations. Compos Sci Technol 2021; 207: 108694.

[11] He Q, Ye L, Kinloch AJ, Wang H, Yin B. Characterisation of fusion bonding between filaments of thin 3D printed polyamide 6 using an essential work of fracture method. J Mater Sci 2021; 56: 2777-94.

[12] Chen Y, Ye L. Designing and tailoring effective elastic modulus and negative Poisson's ratio with continuous carbon fibres using 3D printing. Compos Part A 2021; 150: 106625.

[13] Chen Y, Ye L. Topological design for 3D-printing of carbon fibre reinforced composite structural parts. Compos Sci Technol 2021; 204: 108644.

[14] Chen Y, Ye L, Zhang YX, Fu KK. Compression behaviour of 3D-printed CF/PA metamaterials: Experiment and modelling. Int J Mech Sci 2021; 206: 106634.

[15] Matthews FL, Rawlings RD. 'Composite Materials: Engineering and Science'. Chapman and Hall, London, 1994.

[16] Youssef Z, Jacquemin F, Gloaguen D, Guillen R. A multi-scale analysis of composite structures: Application to the design of accelerated hygrothermal cycles. Compos Struct 2008; 82: 302–09.

[17] Kulkarni R, Ochoa O. Transverse and longitudinal CTE measurements of carbon fibers and their impact on interfacial residual stresses in composites, J Compos Mater 2006, 40: 733–54.

[18] Ito T, Suganuma T, Wakashima K. A micromechanics-based analysis for tailoring glass-fiber reinforced thermoplastic laminates with near-zero coefficients of thermal expansion. Compos Sci Technol 2000; 60: 1851–61.

[19] Kelly A, McCartney LN, Clegg WJ, Stearn RJ. Controlling thermal expansion to obtain negative expansivity using laminated composites. Compos Sci Technol 2005; 65: 47–59.

[20] He Q, Ye L, Kinloch AJ. The essential work of fracture method for the characterisation of fusion bonding in 3D printed short carbon-fibre reinforced polyamide 6 thin films. Submitted for publication 2021.

[21] Blaber J. Adair B, Antoniou A. Ncorr: Open-source 2D digital image correlation Matlab software. Exp Mech 2015; 55: 1105–22.

[22] Abaqus® 6.10 Analysis User's Manual. Dassault Systèmes, Simulia Corp., Providence, RI, USA. 2010.

[23] Chen Y, Ye L, Fu KK, Han X. Transition from buckling to progressive failure during quasi-static in-plane crushing of CF/EP composite sandwich panels. Compos Sci Technol 2018; 168: 133–44.

[24] Iragi M, Pascual-González C, Esnaola A, Lopes CS, Aretxabaleta L. Ply and interlaminar behaviours of 3D printed continuous carbon fibre reinforced thermoplastic laminates: effects of processing conditions and microstructure. Additive Manuf 2019; 30: 100884.

[25] Saeed K, McIlhagger A, Harkin-Jones E, Kelly J, Archer E. Prediction of the in-plane mechanical properties of continuous carbon fibre reinforced 3D printed polymer composites using classical laminated-plate theory. Compos Struct 2021; 259: 113226.

[26] Ibrahim Y, Elkholy A, Schofield JS, Melenka GW, Kempers R. Effective thermal conductivity of 3D-printed continuous fiber polymer composites. Advanced Manufacturing: Polym & Compos Sci 2020; 6: 17–28.

[27] Li F, Sun JY, Xie HL, Yang K, Zhao XF. Thermal deformation of PA66/carbon powder composite made with fused deposition modeling. Materials 2020; 13: 519-33.